Lattice of Passages Connecting Membranes

Thierry Charitat, B. Fourcade

Lattice of Passages Connecting Membranes

T. Charitat and B. Fourcade (*,**)

Institut Laue Langevin, and Maison des Magistères Jean Perrin, C.N.R.S.,
25 avenue des Martyrs, B.P. 166, 38042 Grenoble, Cedex 09, France

(Received 1 August 1996, revised 20 September 1996, accepted 7 October 1996)

PACS.82.70.-y – Disperse systems
PACS.02.40.-k – Geometry, differential geometry, and topology
PACS.68.15.+e – Liquid thin films

Abstract. — Lattices of passages connecting membranes are frequently observed in a variety of membranous systems. We study their elastic properties within the framework of the curvature energy. Our calculations apply to the vesicle case where the constraints of constant surface and volume determine the shape profile. We concentrate on the physically relevant case of periodic boundary conditions for each cell containing passages, where the lattice parameter is set by the Gaussian bending modulus. It is shown that lattices of passages lack in-plane shear rigidity and we propose this as the basic reason for the strong fluctuations which are observed in experiments. Other compression modes couple to the vesicle shape. Our calculations are based on a detailed analysis of the shape equation. Using the Abrikosov vortex solution we show the analogies between lattices of passages and topological defects.

Résumé. — Les réseaux de passages sont fréquemment observés dans les systèmes de membranes. Nous étudions leurs propriétés élastiques dans le cadre d'une énergie de courbure. Nos calculs s'appliquent aux cas des vésicules pour lesquelles les contraintes de surface et de volume déterminent la forme d'équilibre. Nous nous limitons aux conditions aux frontières périodiques pour chaque cellule qui sont physiquement pertinentes et dont le paramètre de réseau dépend du module de courbure Gaussien. Nous montrons que ces réseaux ne possèdent pas de constante élastique de cisaillement et nous proposons que ceci soit à l'origine des fortes fluctuations observées dans les expériences. Les autres modes sont couplés à la forme déquilibre. Nos calculs font appel à une analyse détaillée des équations de la forme de la vésicule. Utilisant la solution d'Abrikosov pour le réseau de vortex, nous montrons les analogies entre les réseaux de passages et les défauts topologiques.

1. Introduction

Multilamellar membranes connected by passages or necks are observable in many lyotropic systems such as bicontinuous or cubic phases in surfactant-water-oil systems [1–5], membranes of amphiphilic molecules swelled in water, *e.g.* vesicles [6–8], or even in the structure of prolamellar bodies of etioplasts in plant cells [9]. The typical scale of these passages is system

(*) also at the Institut Universitaire de France.
(**) Author for correspondence (e-mail: fourcade@mgstsrv.polycnrs-gre.fr)

dependent, ranging from 100 Å to 1 μm. A common property of all of these systems is that the membrane seen as a thin surface divides the space into two interwoven compartments with a large contact surface between the two subvolumes. In these systems the typical radius of a passage is large with respect to the thickness of the membrane and continuum elasticity theory is valid. In the vesicle case, multilamellar systems can spontaneously swell in water or they can be created by the action of optical tweezers [10]. Direct observations by phase contrast microscopy reveal a simple geometrical picture: The membrane can be schematized as a finite number of slabs, stacked on top of each other, and connected by a periodic array (lattice) of passages [6, 7]. In this paper we concentrate on the vesicle case where the equilibrium shapes result from the interplay of the curvature energy with the constraints of constant surface and constant volume [11, 12].

Passages in lyotropic systems other than vesicles differ in the sense that their thermodynamic properties depend on curvature energy, on steric interactions and on entropy of mixing [1, 3]. For example, Bruisnma [3] has shown that minimal surfaces [13] with lattices of passages have vanishing elastic coefficients in the Helfrich energy. In a more recent paper, Gompper and Goos [14] have demonstrated for two membranes experiencing a mutual interaction potential that the shape of the passages experiences strong fluctuations. The case of the vesicle shape problem is however distinct, since these are closed objects where the constraints of constant volume and constant surface determine the shape profile of minimum energy. For vesicles of small topological genus, the constraints lift the conformal degeneracy of the curvature energy [15–17] and set the elastic constants to non-zero values. This has been demonstrated in the case of toroidal geometry where the hole experiences a small restoring force when it moves off the center [18, 19]. Moreover, previous works on higher topology have shown that vesicles of complex topology have distinctive properties. For genus $g \geq 1$, *i.e.* a torus with at last two holes, the ground state can be degenerate, leading to the so-called conformal diffusion process [20, 21] in a region of the surface-volume phase diagram. A different experimental observation is that the position of the passages fluctuate more strongly than expected for vesicles where thermal fluctuations affect smoothly their shape profile [7]. In this paper we derive from first principles both the shape profile of the passages and the elastic properties of lattices of passages. We show that the lattice has only a weak resistance to in-plane shear stress compared to compression which couples to the shape of the vesicle. In this sense, lattices of passages are liquid like, since the stress tensor is reduced to a scalar.

Our analysis is based on the Helfrich curvature energy [22, 23] for passages connecting stacks of membranes. The first section defines the problem. We will work with periodic boundary conditions to mimic the closed shape of a vesicle. In Section 2 we demonstrate from a general point of view that these boundary conditions are crucial to understanding the curvature energy of lattices of passages. Our discussion is based on analogies with the Abrikosov vortex lattice [24, 25] and it is demonstrated that the line of constant current for the superconductor problems corresponds to the line of constant height for the membrane case. This vortex analogies is pushed further by deriving circuit rules for the two types of passages we define. The results presented in the next two sections show that the curvature energy of lattices can be derived from a matching analysis between an inside solution, which characterizes the inside core of a passage, and an outside solution. We show that the Gaussian bending modulus sets the lattice parameter of the unit cell. We will discuss how the constraints determine precisely the position and the relative diameters. We compute the curvature energy of a passage and we show that non-trivial logarithmic corrections appear. The latter are crucial to understanding the elastic properties which we discuss in the last section. It is shown that lattices of passages have almost no shear rigidity. We propose this as the basic reason for the strong fluctuations observed in the experiments. Other fluctuations of the network corresponding to longitudinal

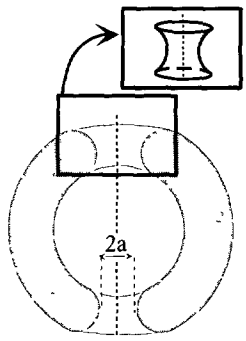

Fig. 1. — Two concentric spherical vesicles with two passages. The shaded area corresponds to the interior volume. The inset represents the profile of a passage. The shape has symmetry of revolution and the inset corresponds to the core of a passage.

phonons are shown to be coupled to the vesicle shape. Using the constraint of constant volume for a long cylinder, we show that lattices of passages increase the effective rigidity of a vesicle. Three Appendices complete this work and contain technical details. We report in this paper on analytical and numerical results. The latter ones have been obtained using the Evolver program [26].

2. The Problem

Let us consider two concentric spherical vesicles as shown in Figure 1. Two passages, one on the north pole and the other one on the south pole, have been opened up. The space is divided into two compartments. The interior volume is defined as the space included between the two spheres: The exterior one includes the inside of the smallest sphere and the outside of the biggest one. One cannot pass from the interior to the exterior without piercing the membrane, so that the volume of the inside is constant. Obviously, this construction can be generalized to an arbitrary number of passages and to an arbitrary even number of spheres. In the limit where the number of passages is large, *i.e.* where the typical radius a of a passage is small with respect to the radii of the spheres, we can schematize the system as an even number of slabs connected by passages organized on a "lattice" with arbitrary symmetry and lattice parameter L . To mimic the closed shape of a vesicle of size R, we apply periodic boundary conditions with $R = \sqrt{N_{\text{cell}}}L$ where N_{cell} is the number of cells.

Each cell contains an arbitrary number N of passages, and consider first the case $N = 1$ with two slabs. For clarity, we will refer to the shape of a membrane of a unit cell simply as the unit cell. Figure 2 shows one example of a square lattice symmetry with periodic boundary conditions in the x and y directions. Obviously, the vesicle size is proportional to the number of unit cells.

As usual for vesicle problems, the constraints of constant surface and constant volume define the variational problem. The latter can be stated as follows: Given the total surface and the total volume of the vesicle, find the minimum energy shape at constant L; then, minimize with respect to L for a given number of passages.

For passages with a finite radius a, the surface and volume of the unit cell depend on the radius a. However, in the limit where $\frac{a}{L} \ll 1$, the leading variation of the reduced volume (see

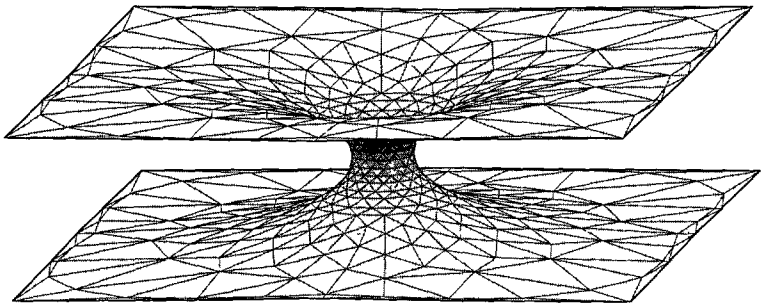

Fig. 2. — One passage where the unit cell has square symmetry. Periodic boundary conditions are applied in the x and y directions. The constraint of a given volume stabilizes the radius a to a non-zero value.

Appendix A for details)

$$\Delta = \frac{V}{S^{\frac{3}{2}}} \tag{1}$$

comes from the volume which scales as

$$V \sim aL^2 \ln\left(\frac{L}{a}\right) \tag{2}$$

Since the surface varies to next order in a as

$$\delta S \sim a^2 \ln\left(\frac{a}{L}\right) \tag{3}$$

we will henceforth study the shape problem at constant L and for a given V.

Concentrating on the simplest model [12] for lipid vesicles, we write the energy per cell as

$$\mathcal{H} = \frac{1}{2}\kappa \int\int (c_1 + c_2)^2 \, \mathrm{d}S + \bar{\kappa} \int\int c_1 c_2 \, \mathrm{d}S \tag{4}$$

where the mean curvature $H \equiv \frac{1}{2}(c_1 + c_2)$ is the average of the two principal curvatures. When working at fixed topology, we will omit the Gaussian curvature term $\bar{\kappa} \oint c_1 c_2 \, \mathrm{d}S$. To account for the constant volume constraint, we introduce a Lagrange multiplier p so that the shape is computed from the minimization of $\mathcal{H} - pV$ at fixed L. Henceforth, we will refer to p as the pressure.

Far from the passages, where all derivatives of the height variable $z(x, y)$ are small, the mean curvature can be approximated by $H \simeq \frac{1}{2}\Delta z$. Thus, to first order in p, we write the Euler equation as

$$\Delta H = \frac{p}{2\kappa} \tag{5}$$

Equation (5) will be solved later. At this point, it is interesting to rederive the variational approach of reference [7] from a new and more general point of view. It will be demonstrated later from first principles that it gives the leading order for the energy per unit cell. However, this approach first developed in reference [7] misses an important point for the fluctuations if the reduced volume constraint is not taken into account.

3. Analogies with Topological Defects

Equation (5) is difficult to solve. Reference [7] has proposed a variational scheme to tackle the problem: A passage costs an energy $\simeq \pi a^2/S$ and, without the constant volume constraint, it shrinks to zero. What the volume constraint does is to keep the radius of a passage at a non-zero value a which depends on the pressure p. Reference [7] has proposed to solve instead of equation (5)

$$\frac{1}{2}\Delta z = H_0 \tag{6}$$

for a given a. This Ansatz will be justified later in the limit $pL^3 \ll 1$. The constant H_0 can be interpreted as a background term which is self-consistently determined by two conditions. First, we require the shape to be periodic. Second, the solution of equation (6) must match a catenoid $z = a\cosh(r/a)$ as $r \to a$. The latter condition implies that a passage is an almost zero curvature surface. Applying Gauss theorem for a periodic network with lattice parameter L gives

$$H_0 = -\frac{\pi a}{S} \tag{7}$$

with

$$z(r) \simeq a\ln(2\frac{r}{L})\ ;\ \frac{r}{L} \ll 1 \tag{8}$$

Reference [7] has numerically shown for a square lattice that equation (6) yields the correct result to leading order in a/L for the problem where a is function of the volume (see Eq. (5)).

This variational approach can be made more explicit if we remark that equation (6) is one of the Ginsburg-Landau equations for the dimensionless order parameter f_0 of a type II superconductor when the magnetic field is equal to its upper critical value H_{c_2}. Let $f_0 = 1$ in the superconducting state and $f_0 = 0$ in the normal state. It will be useful for what follows to write this equation in dimensionless units, since its solution is needed for both the shape $z(x,y)$ and the mean curvature $H(x,y)$. Let κ_s be the ratio of the London penetration depth to the coherence length, then [25]

$$\Delta\ln(f_0^2) + \kappa_s^2 = 0 \tag{9}$$

For the shape problem, we look for a solution

$$z(x,y) = \frac{a}{2}\ln\left(f_0^2(x,y)\right) \tag{10}$$

which matches the shape of a passage located at the origin if

$$f_0(x,y) \simeq r$$

where we have used polar coordinates. Equation (10) will be justified later by matching with an inside solution corresponding to the core of a passage. Thus the problem of passages can be mapped onto the Abrikosov lattice one by rescaling κ_s as κ_s/a. This correspondence can be made one to one, since the lines of constant height for the equilibrium shape problem corresponds to the lines of constant current in the superconductor case. It follows also that the number N of passages per unit cell corresponds to the number of flux lines. This shows that the rule for the conservation of charges which will be rederived later is equivalent to the conservation of the magnetic flux through the superconductor sample.

The general solution of equation (6) for an arbitrary lattice is given in reference [25]. We quote the result without proof (see Appendix A for another useful representation). Let the

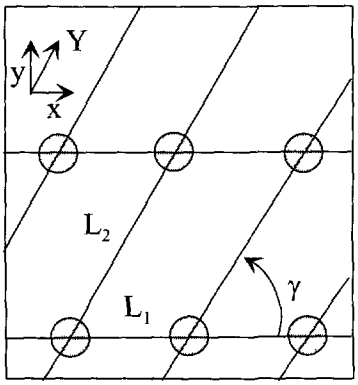

Fig. 3. — Top view of a lattice where γ is the angle between the x- and Y-directions. Under a shear transformation γ varies from $\pi/2$ to $\pi/3$.

unit cell be a parallelogram of length L_1, L_2 and of angle γ as seen in Figure 3. Thus, taking into account the upper and lower leaflet, the total surface of the unit cell is $2L_1L_2\sin(\gamma)$.

The general solution of equation (9) can be written as

$$f_0 = \left| \sum_n C_n \exp\left[\frac{2\pi n\imath}{L_1}(X + Y\cos(\gamma))\right] \exp\left[-\frac{\kappa_s^2}{2}\sin^2(\gamma)\left(Y + \frac{2\pi n}{L_1\kappa_s^2\sin(\gamma)}\right)^2\right]\right| \tag{11}$$

where (X, Y) defines a new coordinate system as

$$x = X + \cos(\gamma)Y \tag{12}$$

$$y = \sin(\gamma)Y \tag{13}$$

To show that the constant curvature value H_0 in equation (7) comes from the periodic boundary conditions, let us assume that the function f_0 is periodic in Y with period L_2. For a cell with N passages, it follows that

$$\kappa_s^2 = \frac{2\pi N}{L_1L_2\sin(\gamma)} \tag{14}$$

where the C_n's are coefficients with

$$C_{n+N} = C_n \exp\left(\frac{2\pi\imath L_2 n}{L_1}\cos(\gamma)\right) \tag{15}$$

The coefficients C_1, C_2... give the positions of the passages within the unit cell which correspond to the zeros of f_0. For $N = 1$, the C_i's depend on an arbitrary constant C_0 as

$$C_n = C_0 e^{\pi\imath n(n-1)\frac{L_2}{L_1}} \tag{16}$$

Taking $\gamma = \frac{\pi}{2}$ gives the square lattice symmetry with passages located at translationally equivalent point of $(0.5, 0.5)$. The triangular lattice is obtained for $\gamma = \frac{\pi}{3}$ where $(X, Y) = \left(\frac{3}{4}, \frac{1}{2}\right)$ gives the locus of one passage. The latter geometry can also be obtained for $N = 2$, since $C_1 = iC_0$ corresponds to a rectangular cell with centering translational symmetry of an equilateral lattice. Equation (14) generalizes equation (7) for arbitrary lattices and for an arbitrary number N of passages per unit cell. It shows that the background term H_0 is

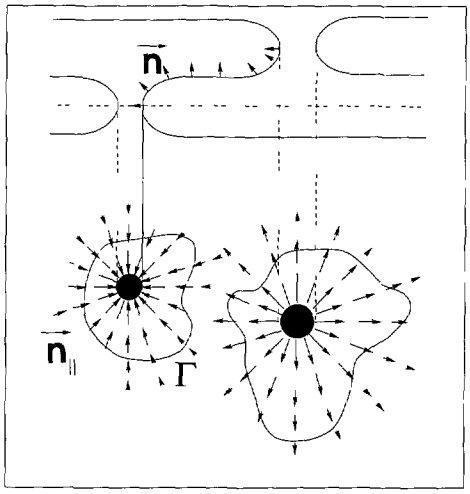

Fig. 4. — Cut view of three slabs connected by two passages. The right passage has outward pointing normal but the left one has inward pointing normal. This convention defines the sign of the passages.

independent of the C_n, since $H_0 = \kappa_s a^{-1}$ where κ_s depends only on the boundary conditions by equation (14). Since H_0 is constant, the energy of such a constant curvature surface does not depend on the actual position of the passages.

It is interesting to push this analogy further by considering the following circuit rule. Near a passage we can approximate

$$z(r) \simeq \pm a \ln\left(\frac{r}{a}\right) \tag{17}$$

where the $\pm$ signs depend on the orientation of the normal with respect to the core of a passage. Figure 4 shows one elementary example where the left passage has an inward pointing normal but where the right one has an outward pointing normal. Let us consider the projection of the normal onto the $z = 0$ plane which reads as

$$\mathbf{n}_{||} = \pm \frac{a}{r} \mathbf{u}_r \tag{18}$$

Gauss s theorem gives that the integral of $\mathbf{n}_{||} \cdot \mathbf{dl}$, where $\mathbf{dl}$ is taken along the outward pointing normal of a path enclosing a passage, is

$$\oint \mathbf{n}_{||} \cdot \mathbf{dl} = \pm 2\pi a \tag{19}$$

The $\pm$ sign in equation (19) depends on the orientation of the normal with respect to the core of a passage. This circuit rule defines the sign of the passage according to the sign in equation (19).

By the same token, we can generalize equation (6) to get the constant background term for a median slab connected to an upper and lower neighbor. Consider a contour which encircles N_+ passages of type + and N_- passages of type −. Assume for simplicity that the radii of the passages are a_+ and a_-. In this case, the flux of the $\mathbf{n}_{||}$ gives $2\pi\,(N_+a_+ - N_-a_-)$ so that it suffices to replace Na by $(N_+a_+ - N_-a_-)$ in equation (7) to account for both types of passages. As a result, surfaces having both type of passages have less curvature energy than the ones for which there is only one type. The case of periodic minimal surfaces [13] corresponds precisely to a geometry where the sum of all signed radii of passages per unit cell is equal to zero.

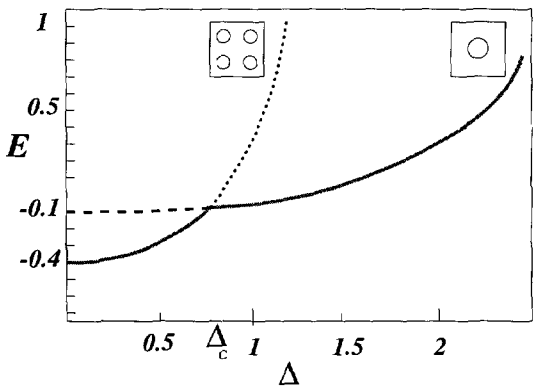

Fig. 5. — Plot of the bending energy as a function of the reduced volume for cells with one and four passages. The bending Gaussian modulus is negative so that the 4 passages solution has the lowest energy at large reduced volumes. The value of the bending Gaussian modulus has been chosen so that $a/L \ll 1$.

According to this approach the stationary shape profile is a constant curvature surface where H_0 is only determined by the condition of periodic boundary conditions. Equation (14) shows that H_0 is independent of the positions of the passages in the unit cell, which are specified by the set of C_n's. Following this variational argument, the passages can be considered as "free particles" with hard-core interaction. The range of this repulsion corresponds to the domain where the curvature cannot be approximated by the Laplacian. We will refer to it as the inside domain and we will show that the size of this domain scales with the radius a in a non trivial way.

However, restoring forces in vesicle problems come both from the variation of the bending energy and from the constant surface-volume constraints. Obviously, moving one passage around the unit cell changes the volume and a restoring force results from this. This point will be demonstrated later, since the distance between the passages is shown to be volume dependent. Thus the concept of isolated passages must be abandoned. Henceforth, we return to the problem with the constraint of constant volume and we show that lattices of passages share another important property with the Abrikosov lattice: Namely, they lack shear rigidity [27].

4. Constant Volume Problem at Fixed L

In the following we will concentrate on the case where passages connect two slabs (see Fig. 2). Adding a small handle to a slab changes the topology. However, we have numerically checked by adding one handle to a unit cell that the minimum bending solution converges to the simplest configuration of two slabs connected by two passages. Handles whose size is of the order of the mesh size cannot be studied and we will discard them.

For the systems we study here, the number of passages per unit cell is determined by the curvature Hamiltonian and by the volume constraint. A positive value for the Gaussian bending modulus means that the minimum energy solution is the one with two parallel slabs. However, it is clear that a negative value of the Gaussian bending modulus cannot create an infinite number of passages because of the volume constraint. This is examplified in Figure 5. The cell with 4 passages has lower energy than the one-passage one at large reduced volumes. We shall see later, so that the triangular and square lattice have almost the same energy for the

same reduced volume so that the threshold value does not depend on the geometry of the unit cell in the small aL^{-1} limit (a rectangular unit cell with centering translational symmetry of an equilateral lattice gives the triangular symmetry. Dividing the rectangle into 4 gives the triangular symmetry again). Therefore, for periodic boundary conditions, the value of the Gaussian bending rigidity sets the lattice parameter and, henceforth, we will work at fixed L.

4.1. THE PERTURBATIVE DOMAIN. — For small volume or for small pressure, *i.e.* $pL^3 \ll 1$, the solution of equation (5) gives a reasonable solution to the shape problem. We have found useful to work also with the representation given in Appendix A. For a square or a triangular lattice with one hole per cell we have, using equation (5) and equation (9) (see Appendix A for details)

$$H(x,y) = \frac{pL^2}{8(\beta-\alpha)} \ln(f_0^2(x,y)) + H_0 \tag{20}$$

where $f_0(x,y)$ can be expressed in terms of the σ function of Weierstrass. The constant H_0 is determined by matching with the inside solution. We will demonstrate later that it yields back equation (7) so that our notation is consistent.

Henceforth, each time we specify a lattice symmetry we will drop the subscript. For example, we will write $f_\triangle$ instead of f_0 for a triangular lattice where $f_\triangle$ reaches its maximum value on the apex of a hexagon and vanishes at point translationally equivalent of the origin. Since we will demonstrate that $pL^2 \ll H_0$, equation (20) implies that the shape $z(x,y)$ is given by equation (10) with corrections to order p. It turns out that these corrections are small when we calculate the volume as in Appendix A.

The two constants α and β in equation (20) are lattice dependent. For a square or a triangular lattice, we have $\alpha = -\beta = \frac{\pi}{4}$ or $\frac{\pi}{2\sqrt{3}}$, respectively. This solution is valid for a lattice where all passages are of the same type. It can be generalized to more general situations. For example, the solution

$$H(x,y) = \frac{\sqrt{3}pL^2}{8\pi} \left[\ln(f_\triangle^2(x,y)) + \ln\left(f_\triangle^2(x-\frac{L}{2},y) \right) \right] + H_0 \tag{21}$$

describes two triangular networks of opposite type, translated in the x direction. The cell contains two passages of opposite type separated by $L/2$. Therefore, this surface has the same symmetry as the Schwartz's H-surface [13].

As usual the Lagrange multiplier p is adjusted to satisfy the constraint of constant volume. In the following we determine p and H_0 as a function of the radius a.

4.2. THE ASYMPTOTIC SOLUTION. — It is shown in Appendix A that the square and triangular lattices are the only ones for which the mean curvature of equation (20) is axisymmetric for $\frac{r}{L} \ll 1$. Therefore, the curvature in the inside domain is an axisymmetric solution of the shape equations. An asymptotic matching between an inside and an outside solution has already been derived for the budding problem [28]. However, in the present case, the Euler equations do not correspond to the Helfrich-Deuling equations for axisymmetric shapes. This is explicitly shown in Appendix B. The problem is that an axisymmetric stationary shape is generated by revolving a curve around the z axis (see Fig. 6). If the surface has the same topology as a sphere, this curve intersects the z axis at a right angle. For case of the passages we study here, this constraint does not exist any more and there is an arbitrary constant c left undetermined in the asymptotic analysis. This constant has to be determined by matching with the perturbative solution.

In Appendix C the asymptotic solution is worked out and it reads as

$$H \simeq -\frac{c}{2}(\ln\left(2\frac{r}{a}\right) - 1) + \frac{p}{\kappa}\frac{r^2}{8} + d \tag{22}$$

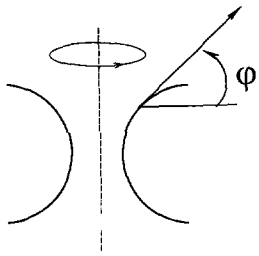

Fig. 6. — Cut view of a surface with symmetry of revolution. The surface is obtained by revolving a curve around the z axis. The angle ϕ between the tangent with respect to the symmetry axis defines the two curvatures of Appendix B.

for $\frac{r}{a} \gg 1$. For a solution with reflection symmetry $z \to -z$, we have $d = 0$ and c is the above mentioned constant which has to be determined by matching.

4.3. The Matching Problem

4.3.1. Two Slabs. — Let us consider the simplest situation where a periodic array of passages connects two slabs. Assuming that the latter are centered at points translationally equivalent to the origin, the pertubative solution behaves as

$$H \simeq H_0 + \frac{pL^2}{8\kappa(\beta - \alpha)} \left(\ln\left(\frac{2r}{L}\right) - (\alpha - \beta)\frac{r^2}{L^2} \right) \tag{23}$$

when $r \to 0$. We assume that equation (22) and equation (23) agree for $\frac{r}{a} \gg 1$ and $\frac{r}{L} \ll 1$. The $\frac{p}{\kappa}\frac{r^2}{8}$ term is automatically matched since it appears in both solutions. Matching the logarithmic term gives

$$c = \frac{pL^2}{4\kappa(\alpha - \beta)} \tag{24}$$

Since the constant is the same in both solutions, we get

$$p \simeq -\frac{8\kappa(\alpha - \beta)H_0}{L^2 \ln(\frac{a}{L})} \quad \frac{a}{L} \ll 1 \tag{25}$$

Finally, matching the radii of curvature gives the constant background term as in equation (6).

The same calculation shows that the leading correction to the pressure given by equation (25) is of order

$$\frac{a}{\left(\ln\left(\frac{a}{L}\right)\right)^2} \tag{26}$$

which is indeed negligible only in the limit of very small ratio aL^{-1}. From the point of view of numerical simulations, only reasonably small values of this ratio can be reliably considered ($aL^{-1} \geq 0.05$). In this regime, these corrections are not that small and it is necessary to adjust numerically the value of p to compare numerical and analytical results. Figure 7 shows an example where p has been optimized so that the asymptotic and perturbative solutions fit the mean curvature obtained with the program Evolver. The numerical value of p differs by 9% from the asymptotic expression given in Appendix C. This shows clearly the existence of an inside domain where the curvature varies rapidly from positive to negative values. The outer

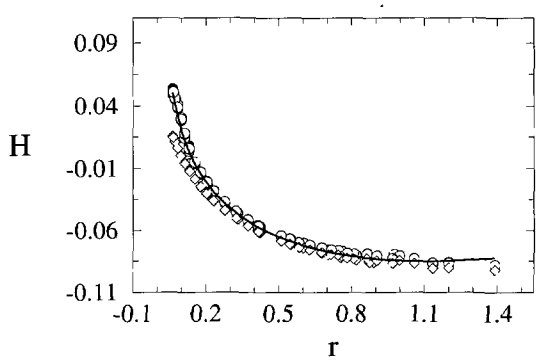

Fig. 7. — Plot of the mean curvature H as a function of the radial distance from the origin. The lattice is a square ($L = 2$). The curve corresponds to the asymptotic analysis of Appendix C. The meaning of the other symbols are as follows: Circles are the numerical data, diamonds correspond to the perturbative expansion. According to equation (26) the matching region is centered at $r = 0.32$. Note that the curvature is slightly non-axisymmetric.

core radius r_c is defined as the distance from the passage above which the next order terms in the asymptotic solution are negligible. From the results of Appendix C, the first correction to equation (22) is $\frac{c}{u^2}\ln(u)$ so that we get

$$r_c = \frac{2}{\pi}\sqrt{aL\ln\left(\frac{L}{a}\right)} \tag{27}$$

As shown in Figure 7 such a value for the overlap domain is again in reasonable agreement with numerical data.

4.3.2. Many Slabs Problem. — Lattices of passages with periodic stacks of membranes in the z-direction give triply periodic minimal surfaces for which the space is divided into two subvolumes V_1 and V_2. For symmetric networks where the numbers of both types of passages are equal $N_+ = N_-$, we have $V_1 = V_2$. However, for $N_+ \neq N_-$, the symmetry $1 \leftrightarrow 2$ does not hold any more and $V_1 \neq V_2$.

The shape profile is uniquely determined by a set of three parameters. These are L (which gives the periodicity in the $x-y$ direction) and d (which gives the periodicity in the z direction). Finally, the third one gives the position of the passages in the unit cell.

To construct such a family of minimal solutions, let us consider the one parameter family of solutions where one passage of type + is centered at the origin with 4 passages of type − The latter are at a distance r_0 of the origin on the diagonal of a square cell (see Fig. 8) so that the shape profile is

$$z(x,y) = \frac{a}{2}\ln\left(\frac{f_\square^2(x,y)}{\prod f_\square^{1/2}(x \pm r_0, y \pm r_0)}\right) \tag{28}$$

Whatever the distance between the two types of passages, the surface is minimal since $\Delta z = 0$. To demonstrate that the constant background $H_0 = 0$, we can expand $f_\square$ near one of its zeros so that the strength of the singular part of z is $a\ln(r)$ near the passage located at the center of the cell: $a_+ = a$. However, one finds $-\frac{a}{4}\ln(r)$ for the passages located along the diagonals, so that $a_- = -\frac{a}{4}$. Summing all contributions gives $H_0 = 0$. It should be noted, however, that the radii a_+, a_- and the relative distance r_0 are not independent parameters. Naive matching

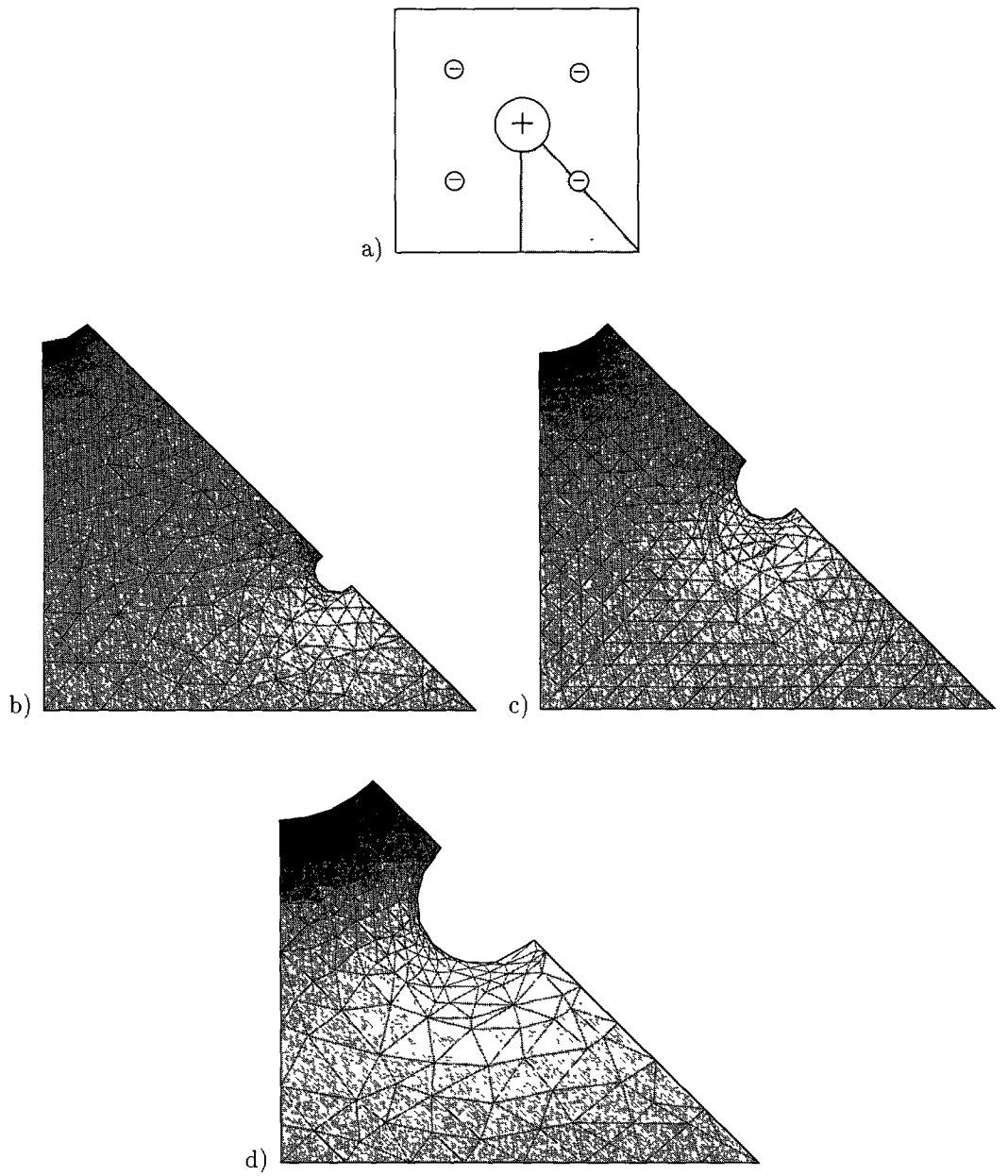

Fig. 8. — a) Top view of a high topology surface where a passage of type + is centered at the origin. The other passages of type − are located on the principal diagonals of the square. The shaded area corresponds to the actual part of the cell which is minimized. b) Varying the relative volume of the two compartments moves the smallest passage off the center and decreases its radius. By definition, the volume encloses the space outside the centered hole. For cases b, c, d one has $\Delta = 0.097, 0.091, 0.079$.

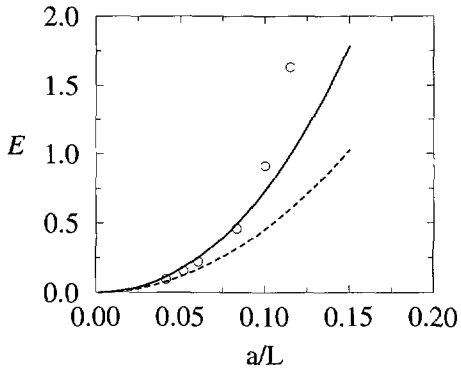

Fig. 9. — Plot of the curvature energy in units of κ_c as a function of a/L. The dashed line corresponds to the first order solution where the curvature is constant ($H_0 = \frac{\pi a}{S}$). The full line corresponds to the logarithmic corrections given by equation (29). Circles correspond to numerical minimization for a triangular lattice.

with a catenoid for the passages yields that the radii decrease as the distance r_0 increases. There is, therefore, a one-parameter family of minimal surfaces of this type.

This degeneracy is broken if we introduce the constraint of a given volume. Figure 8 shows the effect of applying a pressure. It gives an almost constant curvature surface with $H_0 \sim a_+ - 4a_-$ and it selects the distance r_0. As for the minimal case, the small passages move away from the center with decreasing a_-.

4.4. CURVATURE ENERGY. — For the simplest case where two slabs are connected by a lattice of passages we obtain the energy per unit cell as

$$\mathcal{E} \simeq \kappa \frac{4\pi^2 a^2}{S} \left(1 - \frac{2c}{\ln(\frac{a}{L})}\right) \tag{29}$$

where c is a numerical constant which depends on the lattice ($c_\square = 0.60$ and $c_\triangle = 0.68$ for a square and a triangular lattice, respectively). To obtain this expression, we have used equation (20) as well as the asymptotic value of the pressure p given by equation (25). For small radii equation (29) plotted as function of a fits well the numerical data (see Fig. 9). The logarithmic term gives the first correction to the asymptotic regime of equation (7) which is valid in the limit of very small radii. For larger radii, $\frac{a}{L} \geq 0.1$ the scaling regime is no more valid and we have numerically observed that the radius of the passage saturates to $\frac{a}{L} \approx 0.15$ for large pressures.

It is interesting to compare different lattice symmetries for the same number of passages and for the same total surface. The square and triangular lattices have the same area if their lattice parameters are such that

$$L_\square = \left[\frac{\sqrt{3}}{2}\right]^{\frac{1}{2}} L_\triangle \tag{30}$$

Since the volume of each cell depends on the radius a, we use the results of Appendix A to compute $a_\square$ and $a_\triangle$ so that both cells have the same reduced volume $\Delta = S^{-3/2}V$. Taking into account the logarithmic corrections given by equation (29), the energy of the square is

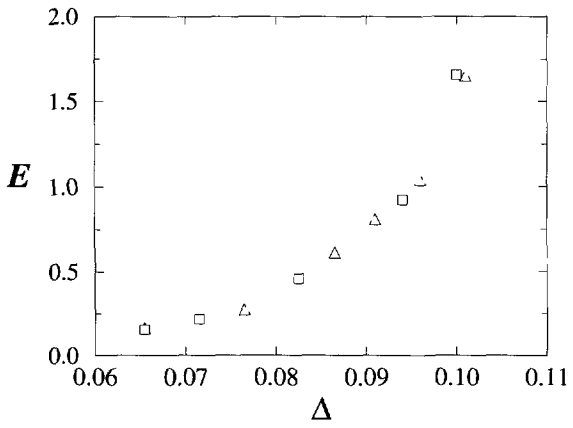

Fig. 10. — Plot of the curvature energy as a function of the reduced volume for the triangular (△) and square symmetry (□).

just above the one with triangular symmetry for the same reduced volume

$$\mathcal{E}_{\square} = \mathcal{E}_{\triangle}\left(1 + \frac{0.16}{\ln\left(\frac{a_{\triangle}}{L_{\triangle}}\right)}\right) \tag{31}$$

This result is valid in the regime $aL^{-1} \ll 1$ where the surface of the unit cell is almost independent of a. For a larger reduced volume, the variation of the surface with the radius a must be taken into account and we have numerically computed the exact reduced volume

$$\Delta = \frac{V(a)}{S(a)^{\frac{3}{2}}} \tag{32}$$

for both types of networks. Figure 10 shows a plot of the curvature energy as a function of the reduced volume where the dependence of the surface on a is taken into account. This shows that the almost degeneracy between the triangular and square symmetry holds even in a regime where aL^{-1} is not small. Such a degeneracy anticipates also the small resistance of these lattices to shear deformations which will be analysed later.

5. Elasticity

As usual linear elasticity theory follows from the long wavelength collective modes. A two-dimensional square lattice has three independent elastic constants but a triangular lattice being more symmetric has only two [24]. They correspond respectively to shear and compression deformations of the lattice.

5.1. Shear Elasticity. — Let us consider first a pure shear deformation where each lattice site experiences a relative displacement $u_x = \epsilon y$ and $u_y = \epsilon x$. Such a transformation leads continuously from a square lattice to a triangular one. In the geometry depicted in Figure 3, this amounts to varying the angle γ with a concomitant rescaling of the lattice parameter L to keep the surface constant. There is however a lower bound for the domain of variation of

the rhombus angle. Its value corresponds precisely to $\gamma = \frac{\pi}{3}$, since the triangular lattice is the lattice of unit surface for which the distance between neighboring sites is maximum.

Since the lengths of each side of the rhombus are kept equal under shear deformations, the volume of an elementary cell can be approximated as

$$V(\gamma) = 2a_\gamma L_\gamma^2 \sin(\gamma) \left(\ln\left(\frac{L_\gamma}{a_\gamma}\right) - c_\gamma \right) \tag{33}$$

where the constant c_γ has to be determined by matching with the inside solution. As shown in Appendix A, the triangular and the square lattice are the only lattices for which the passages have symmetry of revolution. In these cases, $c_\gamma = 0.61\,, 0.68$ for $\gamma = \frac{\pi}{2}\,, \frac{\pi}{3}$. With a passage centered at $z = 0$, the arbitrary constant z_0 for the shape profile $z\,(x, y) \to z(x, y) + z_0$ can only be determined if one assumes that the leading term for the shape corresponds to the catenoid $z \simeq \ln(2r)$ for all γ. In this case, we can numerically determine the unknown constant and compute the volume from $z = a \ln(f_0)$. Monte Carlo integrations give that $c_\gamma \sin(\gamma)$ is almost constant for the ten values of γ we have computed between $\frac{\pi}{3}$ and $\frac{\pi}{2}$ ($c_\gamma \sin(\gamma)$ varies smoothly from 1.17 for $\gamma = \frac{\pi}{3}$ to 1.22 for $\gamma = \frac{\pi}{2}$).

From equation (33) it can be shown the radius a_γ can always be rescaled to maintain the volume constant under shear deformation. Breathing modes are therefore coupled to shear deformations to maintain the volume constraint. As an interesting example, consider the square lattice for which $\gamma = \frac{\pi}{2}$. Small shear deformations change γ as $\gamma = \frac{\pi}{2} + \epsilon$ so that the lattice parameter L increases for the surface to be constant $L_\epsilon = L\left(1 + \frac{\epsilon^2}{4}\right)$. By the same token, the radius a of the passage experiences a shift $a_\epsilon = a\,(1 + \epsilon_a)$ to keep the volume constant. In the very small aL^{-1} limit, one finds using equation (33)

$$\epsilon_a = \frac{\epsilon^2}{4 \ln\left(\frac{a}{L}\right)}$$

Taking into account the logarithmic corrections to the energy (see Eq. (29)), the shift in energy for the square lattice is computed as

$$\Delta\mathcal{E} \simeq -0.4\,\kappa \frac{\pi^2 a^2 \epsilon^2}{L^2 \ln\left(\frac{a}{L}\right)} \tag{34}$$

Therefore, the square lattice is stable with respect to shear deformation.

It is also interesting to estimate the energy barrier between both solutions. Taking $\gamma_{\max} = \frac{1}{2}\left(\frac{\pi}{2} + \frac{\pi}{3}\right)$ for the angle where the energy is maximal gives

$$\Delta\mathcal{E}_{\mathrm{B}} \simeq -\kappa \frac{\pi^2 a^2 \epsilon^2}{L^2 \ln\left(\frac{a}{L}\right)} \tag{35}$$

For reasonable value of aL^{-1}, $\Delta\mathcal{E}$ is small with respect to the thermal energy $k_{\mathrm{B}}T$. This shows, therefore, that low energy excitations corresponding to longitudinal phonons are easily thermally excited.

5.2. Compression Elasticity. — Other modes corresponding to longitudinal phonons are coupled to the shape of the vesicle. The simplest geometry is the one of an infinite cylinder of radius R_0. Consider first the case of a simple cylinder experiencing longitudinal fluctuations of its radius

$$R = R_0 + b_0 + 2b_n \cos(nqR_0 Z) \tag{36}$$

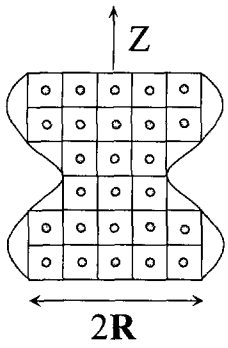

Fig. 11. — Schematic illustration of a cylindrical vesicle where a lattice of passages is wrapped around the symmetry axis. We assume that the passages can flow so that the lattice parameter does not change for a sinusoidal deformation of the cylinder.

where the amplitude of the breathing mode b_0 is chosen so that the inside volume of the cylinder is constant under deformation $b_0 = -\frac{1}{2R_0} b_n^2$. The other constraint of constant surface for the cylinder is usually taken into account by introducing an effective surface tension for the long wavelength deformations [29, 30]. To keep our discussion as simple as possible, we will not address this point and we will consider the problem of a cylinder of length $L_{\rm cyl}$ at constant volume. This constraint is nevertheless necessary to make the cylinder stable in the curvature energy [31]. One finds that the energy per unit length in the Z direction increases as

$$\Delta\mathcal{E}_{\rm c} = \frac{\pi\kappa}{R_0^3}\left(\frac{3}{2} - \frac{1}{2}n^2q^2 + n^4q^4\right)b_n^2 \tag{37}$$

Imagine now that a lattice of passages is wrapped around the cylinder. We assume that the lattice parameter L is such that $L \ll R_0$, such that the results obtained for a periodic lattice with up-down symmetry are valid. Because the shape of the cylinder is deformed, the lattice of passages experiences local deformations including shear and compression of the elementary cell. According to the previous discussion. shear deformations cost very little energy, and we discard them. To evaluate the contribution of the compression modes, we assume that the lattice parameter L scales in the same way as the averaged radius of the cylinder (see Fig. 11). On average, R_0 decreases because of the breathing deformation. Because $R_0 = NL$, the lattice parameter becomes $L(1 + \frac{b_0}{N_{\rm cell}L})$. Therefore, the shift in energy per unit length in the Z direction is

$$\Delta\mathcal{E} = 6\pi^2\kappa\frac{a^2b_n^2}{R_0L^4} \tag{38}$$

In the limit $L \ll R_0$ both energies (Eqs. (38) and (37)) are of the same order. Therefore, the lattice of passages makes the membrane more rigid. As a result, long wavelength deformations for multilamellar vesicles connected by passages should be less pronounced than for non-connected ones.

6. Conclusion

Usual shape fluctuations usually affect the vesicle shape profile smoothly. In this paper, we have shown that lattices of passages lack shear rigidity so that thermal fluctuations will strongly affect the lattice. It is known that long range order is destroyed in two dimensions when forces

are short range. By nature, curvature elasticity is long range and the fluctuations observed in experiments show up on the micrometer scale. The mechanism we have proposed here seems more appropriate to the physics of vesicles.

We have based our analysis on the non-axisymmetric shape equations. The analogies we have drawn with the Abrikosov vortex lattice have shown that passages can be considered as topological defects with a strength equal to the radius of a passage. However, the concept of isolated passages has to be abandoned, since their radii and their distance are not independent parameters. Two passages can differ by the orientation of their normal and we have shown that the curvature depends on the difference between their radii. All these results depend on the periodic boundary conditions which define the unit cell. For the vesicle case, the lattice parameter depends on the Gaussian bending rigidity and on the constraints. However, the symmetry of the unit cell by itself has little influence.

Acknowledgments

We would like to thank Drs. D. Bensimon, X. Michalet, K. Brakke, J. Charvolin and P. Pincus for numerous advices and encouragements. We thank R. Bar-Ziv for helpful discussions.

Appendix A

In this Appendix we give the details for the perturbative solution. For all lattice geometries the solution of equation (6) can be expressed in terms of the Weierstrass σ function [32] where the zeros are located at the lattice sites. Using tabulated properties, it can be shown that

$$\ln[f(x,y)] = \frac{1}{2}\ln\left[|\sigma(z)|^2 e^{(\alpha(z-\bar{z})^2+\beta(z+\bar{z})^2)}\right] \tag{A.1}$$

is doubly periodic with lattice parameter L, where $z \equiv \frac{(x+\imath y)}{L}$, $\bar{z} \equiv \frac{(x-\imath y)}{L}$. The two constants α and β enter into the definition of σ and are lattice dependent. Two cases are of interest: For a square lattice $\alpha = -\beta = \frac{\pi}{4}$ and for a triangular lattice $\alpha = -\beta = \frac{\pi\sqrt{3}}{6}$ In all other cases, $\alpha \neq \beta$. This is important if we look for the leading behavior of f near a vanishing point of σ we will take to be translationally equivalent to the origin. In this case, one finds that

$$\ln[f(x,y)] \simeq \ln(2\frac{r}{L}) - (\alpha-\beta)(\frac{r}{L})^2 + \frac{\alpha+\beta}{\alpha-\beta}(\frac{r}{L})^2\cos(2\theta) \tag{A.2}$$

where r and θ are polar variables. As a result, the square and triangular ones are the only lattices with axisymmetric passages (for a square and for a hexagonal lattice, the first terms which breaks this symmetry are $r^4\cos(4\theta)$ and $r^6\cos(6\theta)$, respectively).

To compute the volume of the unit cell we have found useful to work with Fourier series. We quote the result without proof

$$e^{f_\square^2(x,y)} = d_\square \sum_{n\cdot m}(-1)^{m+n+mn} e^{-\frac{\pi}{2}(m^2+n^2)} \cos\left(\frac{2n\pi}{L}x + \frac{2m\pi}{L}y\right) \tag{A.3}$$

and

$$e^{f_\triangle^2(x,y)} = d_\triangle \sum_{n\cdot m}(-1)^{(mn)} e^{-\frac{\pi}{\sqrt{3}}(m^2+n^2-mn)} \cos\left[\frac{2\pi n}{L}X + \frac{2\pi m}{L}Y - n\frac{\pi}{2}\right] \tag{A.4}$$

As before, the new coordinates system X, Y is defined as

$$x = X + \frac{\sqrt{3}}{2}Y \;;\; y = \frac{1}{2}Y \tag{A.5}$$

where $d_{\square} = 0.348$ and $d_{\triangle} = 0.292$ are two normalization constants such that the leading term of $\ln(f(x,y))$ is $\ln\left(2\frac{r}{L}\right)$. Since the convergence of these series is very rapid, it is easy to compute the volume of each unit cell. Using the leading order for the shape profile

$$z(x,y) = a\left[\ln(f_0(x,y)) + \ln\left(\frac{L}{a}\right)\right] \tag{A.6}$$

we find that the volume is given by

$$V_{\square} \simeq 2aL^2(\ln\left(\frac{L}{a}\right) - c_{\square}) \tag{A.7}$$

$$V_{\triangle} \simeq \sqrt{3}aL^2(\ln\left(\frac{L}{a}\right) - c_{\triangle}) \tag{A.8}$$

where Monte Carlo integration gives $c_{\square} = 0.61 \pm 1$ and $c_{\triangle} = 0.68 \pm 1$. These constants enter into the logarithmic corrections to the curvature energy if the pressure p is given by equation (25).

Finally, the total area can be estimated for a circular cell of radius L for a circular cell of radius L. One finds

$$S(a) = 4\pi L^2\left[1 + \frac{a^2}{L^2}\ln\frac{L}{a}\right] \tag{A.9}$$

so that it varies with the next power of a than the volume.

Appendix B

In this Appendix we generalize the axisymmetric shape equations of Helfrich and Deuling for the general case where the revolving curve is not constrained to intersect the symmetry axis. These equations are first integrals of the variational problem and they depend on an arbitrary constant.

Let us consider a curve which, under rotation around the z-axis, generates an axisymmetric surface. If ϕ (see Fig. 6) is the angle between the normal and oz, the mean curvature at a point at a distance r from the symmetry axis is

$$H = \frac{1}{2}\left(\cos(\phi)\frac{\mathrm{d}\phi}{\mathrm{d}r} + \frac{\sin(\phi)}{r}\right) \tag{B.1}$$

By geometry we have

$$\frac{\mathrm{d}z}{\mathrm{d}r} = -\tan(\phi) \tag{B.2}$$

Including two Lagrange multipliers σ and p for the constraints of constant surface and constant volume, the functional we want to make stationary is given by

$$L = \int_{r=a}^{r=R} \mathcal{L}\,\mathrm{d}r$$

where

$$\mathcal{L} = \kappa\frac{r}{2\cos(\phi)}(2H)^2 + \frac{\sigma r}{\cos(\phi)} + pr^2\tan(\phi) \tag{B.3}$$

In this equation we have chosen the sign of the pressure p in order it coincides with the definition given in the text, and L has been renormalized by 2π. Under variation $z \to z + \epsilon(z)$, where ϵ and $\dot{\epsilon}(z)$ vanish at both end points, ϕ varies as

$$\phi(r) \to \phi(r) - \cos(\phi)^2\frac{\mathrm{d}\epsilon}{\mathrm{d}r} \tag{B.4}$$

Therefore, the first order variation δL is identically zero if

$$\frac{\mathrm{d}}{\mathrm{d}r}\left[\cos(\phi)^2\left(\frac{\partial \mathcal{L}}{\partial \phi} - \frac{\mathrm{d}}{\mathrm{d}r}\frac{\partial \mathcal{L}}{\partial \dot{\phi}}\right)\right] = 0 \tag{B.5}$$

And, as a result, a first integral for the Euler Equations is

$$\frac{\partial \mathcal{L}}{\partial \phi} - \frac{\mathrm{d}}{\mathrm{d}r}\frac{\partial \mathcal{L}}{\partial \dot{\phi}} = \frac{c}{\cos(\phi)^2} \tag{B.6}$$

where c is an arbitrary constant. As shown by Zheng and Liu [33], the condition for the curve to be regular at the intersection point with the symmetry axis implies that $c = 0$. To see this, approximate $z \cong \frac{r^2}{2R}$ near this point where R is the radius of curvature on the symmetry axis. We have $\phi \cong \frac{r}{R}$ as $r \to 0$. Expanding equation (B.6) in the limit $r \to 0$ demonstrates that $c = 0$.

However, for a solution which does not intersect the z-axis, such as for the passages we study here, the constant c is arbitrary. Noticing that the curvature c_p and c_m along the parallel and meridian cross-section are respectively

$$c_\mathrm{p} = \frac{\sin(\phi)}{r} \; ; \; c_\mathrm{m} = \cos(\phi)\frac{\mathrm{d}\phi}{\mathrm{d}r} \tag{B.7}$$

equation (B.6) can be rewritten as

$$\frac{\mathrm{d}}{\mathrm{d}r}\left[c_\mathrm{p} + c_\mathrm{m}\right] = \frac{r}{2\left(1 - r^2 c_\mathrm{p}^2\right)}\left(c_\mathrm{p}\left(c_\mathrm{p}^2 - c_\mathrm{m}^2\right) + \frac{1}{\kappa}\left(p + 2\sigma c_\mathrm{p}\right)\right) + \frac{c}{r\left(1 - r^2 c_\mathrm{p}^2\right)} \tag{B.8}$$

with

$$\frac{\mathrm{d}c_\mathrm{p}}{\mathrm{d}r} = \frac{c_\mathrm{m} - c_\mathrm{p}}{r} \tag{B.9}$$

equation (B.8) and equation (B.9) generalize the Helfrich-Deuling equations for axisymmetric vesicle shapes. In general, $c \neq 0$ and its value has to be determined by matching with the solution valid far from the core of the passage.

Appendix C

In this Appendix we derive the asymptotic expansion to leading order in the pressure. This solution is valid near the core of a passage and it is independent of the symmetry of the lattice.

Let us consider the axis-symmetric shape equations we have derived in the preceding Appendix. To match with the perturbative expansion, we take $\sigma = 0$ but $p \neq 0$. For a passage with radius a, we look for a solution of the type

$$c_\mathrm{p}(u) + c_\mathrm{m}(u) = \sum_{n \geq 1}\left(\frac{p}{\kappa}\right)^n \epsilon^{(n)}(u) \tag{C.1}$$

where all coordinates have been scaled as $r \to u \equiv \frac{r}{a}$ Since the sign of the mean curvature has to agree with the one given for the perturbative regime we have

$$H = \frac{1}{2}\left(c_\mathrm{p}(u) + c_\mathrm{m}(u)\right) \tag{C.2}$$

For a catenoid

$$c_\mathrm{p} = \frac{1}{au^2} \; ; \; c_\mathrm{m} = -\frac{1}{au^2},$$

so that the first $n = 0$ term does not appear in equation (C.1). As a result, the curvature along the parallel cross-section can be expressed as

$$c_{\mathrm{p}}(u) = \frac{1}{au^2} + \sum_{n\geq 1} \left(\frac{p}{\kappa}\right)^n \frac{1}{u^2} \int_1^u x\epsilon^{(n)}(x)\,\mathrm{d}x \tag{C.3}$$

where, by definition, $ac_{\mathrm{p}}(u = 1) = 1$. Because c_{p} scales as $\frac{L}{a} \gg 1$, we can linearize the Euler equation (B.8) to first order in p as

$$\frac{\mathrm{d}\epsilon^{(1)}(u)}{\mathrm{d}u} = \frac{a^2u^3}{u^2-1}\left[\frac{\epsilon^{(1)}(u)}{a^2u^4} + \frac{1}{2}\right] + \frac{c\kappa}{p}\frac{u}{u^2-1} \tag{C.4}$$

where we have assumed $\frac{p^2}{a} \ll p$.

In general the unknown constant c has to be evaluated by matching with the outside solution obtained by straight perturbation. Anticipating with what follows, one has $c \sim p$ so that the last term is of the same order as the first ones. The general solution of this differential equation can now be obtained as

$$\epsilon^{(1)}(u) = B(u)\frac{\sqrt{u^2-1}}{u} \tag{C.5}$$

with

$$B(t) = \kappa\frac{c}{p}(t - \coth(t)) + \frac{a^2}{4}\left(\frac{3}{2}t + \frac{1}{4}\sinh(2t) - \coth(t)\right) + d \tag{C.6}$$

where we define

$$u = \cosh(t)$$

For a solution symmetric with respect to the $z = 0$ plane, we have $d = 0$. To demonstrate this, recall that by equations (B.2) and (B.7)

$$\frac{\mathrm{d}z}{\mathrm{d}s} = \sin(\phi) \simeq \sqrt{1 - \frac{1}{u^2}} \tag{C.7}$$

Therefore,

$$\sqrt{u^2-1}$$

gives in equation (C.5) the odd term $d = c_3$ in the expansion of the mean curvature $H(s) = c_2s^2 + c_3s^3$ as a function of s ($s = 0$ refers to the core of the passage). For a symmetric equilibrium shape, $H(s)$ is invariant under the change $s \to -s$, so that $d = 0$.

When $u \gg 1$, one moves away from the core of the passage and the mean curvature $H(s)$ behaves as

$$H \simeq -\frac{c}{2}(\ln\left(2\frac{r}{a}\right) - 1) + \frac{p}{\kappa}\frac{r^2}{8} + O\left(\frac{p^2}{a}\right) \tag{C.8}$$

It is also of interest to know the asymptotic behavior of the shape $z(r)$. Using equation (C.3) we get

$$rc_{\mathrm{p}}(r) \simeq \frac{a}{r} + \frac{c}{2\kappa}r\ln\left(\frac{r}{a}\right) \tag{C.9}$$

Integrating again equation (B.2) gives the result

$$z(r) \simeq a\ln\left(\frac{r}{a}\right) + \frac{cr^2}{4}\ln\left(\frac{r}{a}\right) \tag{C.10}$$

This asymptotic behavior is used in the text to match the inside solution of equations (C.5) and (C.6) with the one obtained by perturbation.

References

[1] Roux D., Coulon C. and Cates M.E., *J. Phys. Chem.* **96** (1992) 4174.
[2] Porte G., *J. Phys. Cond. Matter* **4** (1992) 8649.
[3] Bruinsma R., *J. Phys. II France* **2** (1992) 425.
[4] Morse D., *Phys. Rev. E* **50** (1994) 2423.
[5] Golubovic L., *Phys. Rev. E* **50** (1994) 2419.
[6] Harbich R.M., Servuss W. and Helfrich W., *Z. Naturforsch. A* **33** (1978) 1013.
[7] Michalet X., Bensimon D. and Fourcade B., *Phys. Rev. Lett.* **72** (1994) 168.
[8] Michalet X., Ph.D. thesis, Paris VII, 1994, unpublished.
[9] Gunning M.E.S. and Steer M.W., Ultrastructure and the Biology of Plant Cells, 1st ed. (Edward Arnaold, Ltd., London, 1975).
[10] Bar Ziv R., private communication.
[11] Lipowsky R., *Nature* **349** (1991) 475.
[12] Structure and Dynamics of Membranes - from Cells to Vesicles, R. Lipowsky and E. Sackmann, Eds. (Elsevier, Amsterdam, 1995).
[13] Dierkes U., Hildebrandt A., Küster A. and Wohlrab O., Minimal Surfaces (Springer Verlag, Berlin Heidelberg, 1992).
[14] Gomper G. and Goos J., *J. Phys. II France* **5** (1995) 621.
[15] Willmore T., Total curvature in Riemannian geometry, 1st ed. (Ellis Horwood, Ltd., New York-Brisbane-Chichester-Toronto, 1982).
[16] Duplantier B., *Physica A* **168** (1990) 179.
[17] Seifert U., *Phys. Rev. Lett.* **66** (1991) 2404.
[18] Fourcade B., *J. Phys. II France* **2** (1992) 1705.
[19] Michalet X. and Bensimon D., *J. Phys. II France* **5** (1995) 263.
[20] Michalet X. and Bensimon D., *Sciences* **269** (1995) 666.
[21] Jülicher F., Seifert U. and Lipowsky R., *Phys. Rev. Lett.* **71** (1993) 452.
[22] Canham P., *J. Theor. Biol.* **26** (1970) 61.
[23] Helfrich W., *Z. Naturforsch. C* **28** (1973) 693.
[24] Chaikin P. and Lubensky T., Principles of Condensed Matter Physics, 1st ed. (Cambridge University Press, Cambridge, 1995).
[25] Saint-James G., Sarma D. and Thomas E., Type II Superconductivity, 1st ed. (Pergamon Press, Oxford, 1969).
[26] Brakke K., *Experimental Mathematics* **1** (1992) 141, evolver is a public domain program available at geom.umn.edu.
[27] de Gennes P. and Matricon J., *Rev. Mod. Phys.* **36** (1965) 45.
[28] Fourcade B., Miao L., Rao M., Wortis M. and Zia R., *Phys. Rev. E* **49** (1994) 5276.
[29] Milner S. and Safran S., *Phys. Rev. A* **36** (1987) 4371.
[30] Seifert U., *Z. Phys. B* **97** (1995) 299.
[31] Ou-Yang Z.C. and Helfrich W., *Phys. Rev. A* **39** (1989) 5280.
[32] Knupp K., Theory of functions (Dover, New York, 1947).
[33] Wei-Mou Zheng and Jixing Liu, *Phys. Rev. E* **48** (1993) 2856.